Proceedings of the 28th IEEE
EMBS Annual International Conference
New York City, USA, Aug 30-Sept 3, 2006

A High-Resolution Anisotropic Finite-Volume Head Model for EEG Source Analysis

Michael J. D. Cook, *Student Member, IEEE* and Zoltan J. Koles, *Member, IEEE*

***Abstract*—Solution of the electroencephalogram (EEG) forward problem in a realistic head model is necessary for accurate source analysis. Realistic head models are usually derived from volumetric magnetic resonance images that provide a voxel resolution of about 1 mm^3. The availability of an electrical head model with this resolution would therefore be extremely advantageous. Head models with resolution in the millimeter range that incorporate the anisotropic properties of their elements have been formulated with the finite element method (FEM). However, these FEM models are fraught with complications related to irregular grids and meshes, along with the incumbent segmentation problems. Presented here is a finite volume method (FVM) formulation of the realistic head model in cubic elements that can ameliorate some of these problems, can incorporate tissue anisotropy, and is both physically intuitive and simple to implement.**

I. Introduction

Electroencephalogram (EEG) source analysis is a powerful tool for studying brain (dys)function. In particular, it can be used to more accurately localize the source of seizures in epilepsy patients. However, the utility of EEG source analysis is ultimately determined by the accuracy of the available head model. A high-resolution, realistic, patient-specific head model is, therefore, a vital component of EEG source analysis.

In this work, we present an approach to head modeling that is based on the finite volume method (FVM). It utilizes a grid of millimeter-level cubic volume elements (voxels) that, in terms of tissue conductivities, can be individually anisotropic. This suggests that, in theory at least, magnetic resonance (MR) images could be mapped directly, voxel by voxel, into the electrical head model. Anisotropy is an essential inclusion in any realistic head model as it is well known that tissues in the head, such as skull and brain white matter, can be quite anisotropic electrically [1]. It is exciting to note that estimates of tissue conductivity can now be obtained directly using an MR imaging modality called diffusion tensor imaging (DTI) [1]. Therefore, in addition to providing patient-specific data, DTI could, with our model, potentially eliminate the need for segmentation of MR images into the different tissue compartments. This could also eliminate the gridding and meshing problems associated with the finite element and boundary element methods.

With 1 mm^3 resolution, our FVM head model would consist of more than 4 million voxels for a normal adult head. However, the domain-decomposition problem is fairly simple and the resulting system (or stiffness) matrix is very sparse. Also, due to the symmetric, positive definite nature of the system matrix, fast iterative techniques can be used to solve the forward EEG problem efficiently in terms of both computer memory and computation time [2].

It should be noted that comparable numerical formulations have been applied to oil reservoir simulations in the past [3-7]. However, we believe this is the first time this particular numerical formulation has been applied to a bioelectric problem such as EEG source analysis. In our opinion, one of the main attractions of our formulation is that it is very straightforward and physically intuitive.

II. Finite Volume Method Formulations

The relationship between electric potential and current at each point in the head model for the EEG source analysis problem is governed by Poisson's equation

$$-\nabla\bullet(\boldsymbol{\sigma}\nabla\phi) = I_V, \tag{1}$$

where $\boldsymbol{\sigma}$ is the conductivity tensor, ϕ is the electric potential, and I_V is the current source. The Neumann boundary condition on the outer surface of the head requires that

$$(\boldsymbol{\sigma}\nabla\phi)\bullet\hat{\mathbf{n}} = 0, \tag{2}$$

where $\hat{\mathbf{n}}$ is the unit normal vector to the outer surface of the head.

For the FVM, a regular grid of cubic voxels is used to discretize the physical domain. Conductivity is defined at the center of the voxels, and is assumed to be piecewise constant over each voxel, whereas electric potentials are defined at nodes on the voxel vertices. To discretize (1), it is first integrated over a control volume at every node. The control volumes are defined as cubic volumes the same size as the grid voxels and are centered on each node. After applying the divergence theorem, the governing equation is now

$$-\oint_S \boldsymbol{\sigma}\nabla\phi\bullet d\mathbf{S} = \int_V I_V\, dV, \tag{3}$$

where V is the control volume that surrounds the node of interest and S is the surface of the control volume. It is important to note that the boundary conditions are automatically handled by the FVM, with no current flowing from the head into surrounding air voxels. Also, the FVM is

Manuscript received April 24, 2006. This work was supported in part by the Natural Sciences and Engineering Research Council (NSERC) of Canada, Alberta Ingenuity, and Informatics Circle of Research Excellence (iCORE).

M. J. D. Cook and Z. J. Koles are with the Electrical and Computer Engineering Department, University of Alberta, Edmonton, AB, T6G 2V4 Canada (phone: 780-492-9463; fax: 780-492-1811; e-mail: mcook@ualberta.ca, z.koles@ualberta.ca).

flux continuous, meaning that current continuity is satisfied over the entire computational domain.

For clarity, the finite volume solution to (1) will be derived in 2D. This can then be easily extended to the 3D case.

A. 2D Formulation

For the 2D case, the voxels and control volumes are both 2D square elements with dimensions $h \times h$, as shown in Fig. 1. In 2D, the conductivity tensor for each voxel can be represented by a symmetric 2×2 matrix

$$\boldsymbol{\sigma} = \begin{bmatrix} \sigma^{xx} & \sigma^{xy} \\ \sigma^{xy} & \sigma^{yy} \end{bmatrix}. \tag{4}$$

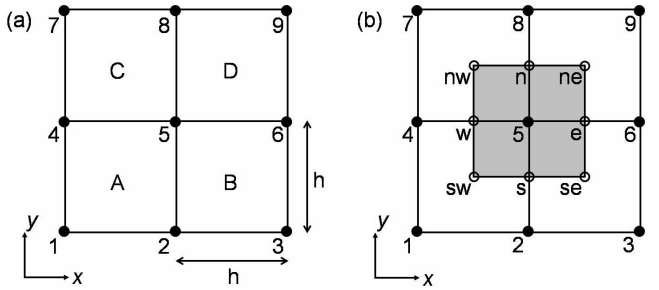

Fig. 1. (a) Grid used for the 2D FVM formulation, with voxels denoted by letters A through D and nodes denoted by numbers 1 through 9. (b) 2D grid with control volume indicated by the shaded area.

To discretize (3) for node 5, the surface integral can be written as

$$-\left(\left(\boldsymbol{\sigma}\nabla\phi\bullet\mathbf{S}^x\right)_e - \left(\boldsymbol{\sigma}\nabla\phi\bullet\mathbf{S}^x\right)_w + \left(\boldsymbol{\sigma}\nabla\phi\bullet\mathbf{S}^y\right)_n - \left(\boldsymbol{\sigma}\nabla\phi\bullet\mathbf{S}^y\right)_s\right) = I_V h^2, \tag{5}$$

where $\mathbf{S}^x$ and $\mathbf{S}^y$ are the normal vectors for the faces of S and are defined as $\mathbf{S}^x = \begin{bmatrix} h & 0 \end{bmatrix}^T$ and $\mathbf{S}^y = \begin{bmatrix} 0 & h \end{bmatrix}^T$.

Evaluating (5), each of the terms on the left side can be physically interpreted as the current flowing out through the faces of the control volume, while the term on the right hand side is the total source current originating in the control volume. The terms in (5) can be further discretized by calculating the current flowing through each face of V. As a sample calculation, the current through face e will be calculated. This current can first be split into a sum of two currents, one in element B and one in element D, as shown in Fig. 2, such that

$$\left(\boldsymbol{\sigma}\nabla\phi\bullet\mathbf{S}^x\right)_e = J_e^B + J_e^D = \boldsymbol{\sigma}_B\nabla\phi_e^B\bullet\left(\frac{\mathbf{S}^x}{2}\right) + \boldsymbol{\sigma}_D\nabla\phi_e^D\bullet\left(\frac{\mathbf{S}^x}{2}\right), \tag{6}$$

where J_e^B and J_e^D are the currents through face e in elements B and D respectively, and $\nabla\phi_e^B$ and $\nabla\phi_e^D$ are the electric potential gradients at point e in elements B and D respectively. The gradients in (6) can be approximated as

$$\nabla\phi_e^B = \begin{bmatrix} (\phi_6 - \phi_5)/h \\ (\phi_e - \phi_{se})/(h/2) \end{bmatrix}, \tag{7}$$

$$\nabla\phi_e^D = \begin{bmatrix} (\phi_6 - \phi_5)/h \\ (\phi_{ne} - \phi_e)/(h/2) \end{bmatrix}, \tag{8}$$

where $\phi_e = (\phi_5 + \phi_6)/2$, $\phi_{se} = (\phi_2 + \phi_3 + \phi_5 + \phi_6)/4$, and $\phi_{ne} = (\phi_5 + \phi_6 + \phi_8 + \phi_9)/4$. Substituting (7) and (8) into (6) and simplifying the expression yields the following equation for the total current through face e

$$\begin{aligned}\left(\boldsymbol{\sigma}\nabla\phi\bullet\mathbf{S}^x\right)_e = {} & \frac{\left(\sigma_B^{xx} + \sigma_D^{xx}\right)}{2}(\phi_6 - \phi_5) \\ & + \frac{\sigma_B^{xy}}{4}\left[(\phi_5 + \phi_6) - (\phi_2 + \phi_3)\right] \\ & + \frac{\sigma_D^{xy}}{4}\left[(\phi_8 + \phi_9) - (\phi_5 + \phi_6)\right].\end{aligned} \tag{9}$$

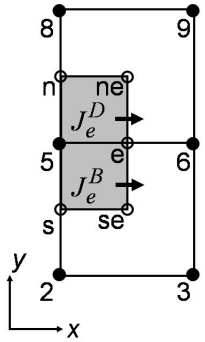

Fig. 2. Current through face e can be split into two components, one in element B and one in element D.

Repeating this process for each face of the control volume enables (5) to be simplified as

$$\sum_{i=1}^{9} A_i\phi_i = I_V h^2, \tag{10}$$

where the coefficients, A_i, are given by

$$A_1 = -\frac{1}{2}\sigma_A^{xy}, \tag{11}$$

$$A_2 = -\frac{1}{2}\left(\sigma_A^{yy} + \sigma_B^{yy}\right), \tag{12}$$

$$A_3 = \frac{1}{2}\sigma_B^{xy}, \tag{13}$$

$$A_4 = -\frac{1}{2}\left(\sigma_A^{xx} + \sigma_C^{xx}\right), \tag{14}$$

$$A_6 = -\frac{1}{2}\left(\sigma_B^{xx} + \sigma_D^{xx}\right), \tag{15}$$

$$A_7 = \frac{1}{2}\sigma_C^{xy}, \tag{16}$$

$$A_8 = -\frac{1}{2}\left(\sigma_C^{yy} + \sigma_D^{yy}\right), \tag{17}$$

$$A_9 = -\frac{1}{2}\sigma_D^{xy}, \tag{18}$$

$$A_5 = -\left(\sum_{\substack{i=1 \\ i \neq 5}}^{9} A_i \right). \tag{19}$$

B. 3D Formulation

For the 3D case, the voxels and control volumes are both cubic elements with dimensions $h \times h \times h$. Using the same reasoning as employed in the 2D case, a discrete version of (3) can be developed for node 10 in the 3D grid shown in Fig. 3. In 3D, the conductivity tensor for each voxel can be represented by a symmetric 3×3 matrix

$$\boldsymbol{\sigma} = \begin{bmatrix} \sigma^{xx} & \sigma^{xy} & \sigma^{xz} \\ \sigma^{xy} & \sigma^{yy} & \sigma^{yz} \\ \sigma^{xz} & \sigma^{yz} & \sigma^{zz} \end{bmatrix}. \tag{20}$$

The discrete version of (3) again results in an expression for which the current through each face of the control volume is calculated. However, in 3D this current is split into the sum of four currents, since each control volume face consists of parts of four voxels. Therefore, the resultant equation for node 10 is

$$\sum_{i=1}^{19} A_i \phi_i = I_V h^2, \tag{21}$$

where the coefficients, A_i, are given by:

$$A_1 = -\frac{1}{4}\left(\sigma_A^{yz} + \sigma_B^{yz} \right), \tag{22}$$

$$A_2 = -\frac{1}{4}\left(\sigma_A^{xz} + \sigma_C^{xz} \right), \tag{23}$$

$$A_3 = -\frac{1}{4}\left(\sigma_A^{zz} + \sigma_B^{zz} + \sigma_C^{zz} + \sigma_D^{zz} \right), \tag{24}$$

$$A_4 = \frac{1}{4}\left(\sigma_B^{xz} + \sigma_D^{xz} \right), \tag{25}$$

$$A_5 = \frac{1}{4}\left(\sigma_C^{yz} + \sigma_D^{yz} \right), \tag{26}$$

$$A_6 = -\frac{1}{4}\left(\sigma_A^{xy} + \sigma_E^{xy} \right), \tag{27}$$

$$A_7 = -\frac{1}{4}\left(\sigma_A^{yy} + \sigma_B^{yy} + \sigma_E^{yy} + \sigma_F^{yy} \right), \tag{28}$$

$$A_8 = \frac{1}{4}\left(\sigma_B^{xy} + \sigma_F^{xy} \right), \tag{29}$$

$$A_9 = -\frac{1}{4}\left(\sigma_A^{xx} + \sigma_C^{xx} + \sigma_E^{xx} + \sigma_G^{xx} \right), \tag{30}$$

$$A_{11} = -\frac{1}{4}\left(\sigma_B^{xx} + \sigma_D^{xx} + \sigma_F^{xx} + \sigma_H^{xx} \right), \tag{31}$$

$$A_{12} = \frac{1}{4}\left(\sigma_C^{xy} + \sigma_G^{xy} \right), \tag{32}$$

$$A_{13} = -\frac{1}{4}\left(\sigma_C^{yy} + \sigma_D^{yy} + \sigma_G^{yy} + \sigma_H^{yy} \right), \tag{33}$$

$$A_{14} = -\frac{1}{4}\left(\sigma_D^{xy} + \sigma_H^{xy} \right), \tag{34}$$

$$A_{15} = \frac{1}{4}\left(\sigma_E^{yz} + \sigma_F^{yz} \right), \tag{35}$$

$$A_{16} = \frac{1}{4}\left(\sigma_E^{xz} + \sigma_G^{xz} \right), \tag{36}$$

$$A_{17} = -\frac{1}{4}\left(\sigma_E^{zz} + \sigma_F^{zz} + \sigma_G^{zz} + \sigma_H^{zz} \right), \tag{37}$$

$$A_{18} = -\frac{1}{4}\left(\sigma_F^{xz} + \sigma_H^{xz} \right), \tag{38}$$

$$A_{19} = -\frac{1}{4}\left(\sigma_G^{yz} + \sigma_H^{yz} \right), \tag{39}$$

$$A_{10} = -\left(\sum_{\substack{i=1 \\ i \neq 10}}^{19} A_i \right). \tag{40}$$

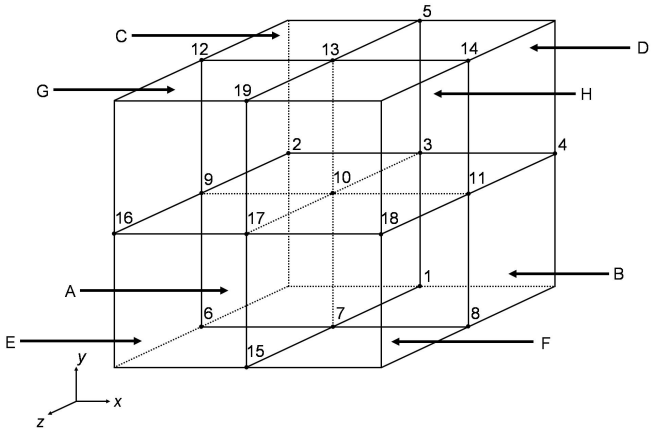

Fig. 3. Grid used for the 3D FVM formulation, with voxels denoted by letters A through H and nodes denoted by numbers 1 through 19.

III. Discussion

Decomposing an entire computational domain of N nodes into N discrete equations results in a system of equations of the form

$$\mathbf{A}\mathbf{v} = \mathbf{i}, \tag{41}$$

where $\mathbf{A}$ is an $N \times N$ system (or stiffness) matrix, $\mathbf{v}$ is an $N \times 1$ vector containing the electric potentials, ϕ_i, at every node, and $\mathbf{i}$ is an $N \times 1$ column vector containing any nodal source currents. The system matrix is symmetric and, after a reference node is chosen, it is also positive definite. Consequently, the system of equations can be solved using fast iterative techniques such as the preconditioned conjugate gradient (PCG) method or the algebraic multigrid method.

Upon evaluating the coefficients for the 2D and 3D cases, it can be seen that they are similar to those derived by the finite difference method in [8]. In fact, with some rearrangement of the equations, the coefficients here and in [8] can be shown to be identical. The derivation presented in this work, however, is physically intuitive and considerably simpler.

IV. Simulations

A. Analytic Spherical Head Model

To compare our FVM formulation to an analytic spherical head model [9], a three-shell anisotropic spherical head model was used in solving the EEG forward problem. As usual, the shells in the head model represented the brain, skull, and scalp, and had radii of 8.0, 8.6, and 9.2 cm respectively. The current source was modeled as a dipole located at a distance of 7.4 cm from the center and oriented in the radial direction. The FVM head model consisted of roughly 3.2 million 1 mm^3 voxels and the forward problem was solved using the PCG method. Fig. 4 compares the potentials on the scalp and shows that there is good agreement between the numerically and analytically calculated values.

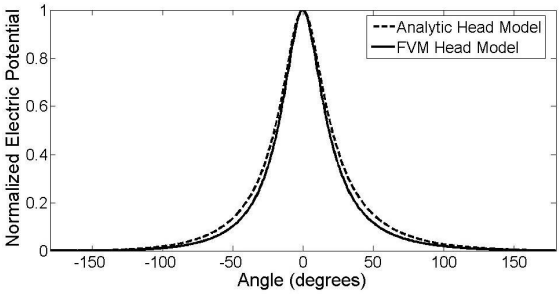

Fig. 4. Comparison of scalp potentials from the analytic and FVM head models. Electric potentials have been normalized to a value of 1.

B. Effect of Anisotropic Conductivity

To illustrate of the effects of anisotropic conductivity, the EEG forward problem was solved using our FVM formulation on the same three-shell spherical head model, with a dipole placed at the center of the sphere. The tissue compartments were first assigned isotropic conductivities and then, for the anisotropic case, the brain compartment's conductivity was increased by a factor of two only in the radial direction. The resulting electric potential distributions are shown in Fig. 5. The contours marked by the arrows in Fig. 5(a) and (b) indicate the same isopotential line relative to the peak positive potential obtained in each solution. These qualitative results are as expected, since the potentials drop off more slowly in the direction of higher conductivity. These results are also in agreement with [1], in that the effects of anisotropy should not be neglected.

V. Conclusion

In this work, we have presented a high-resolution anisotropic FVM head model for EEG source analysis. We employ a regular grid of millimeter-level cubic voxels that, in theory, could allow a direct mapping of MR images into the electrical head model. In addition, compared to the finite element and boundary element methods, our formulation of the head model is physically intuitive, it is relatively simple to set up, and could all but eliminate the very serious problems in the other methods related to image segmentation, grid generation, and meshing. The resultant system matrix, in addition to being both symmetric and positive definite, is more sparse than that resulting from the other methods. These are extremely desirable properties as methods are now available to solve very large systems of this type [2]. In the future, we intend to apply our formulation to human images obtained from both DTI and structural MR data.

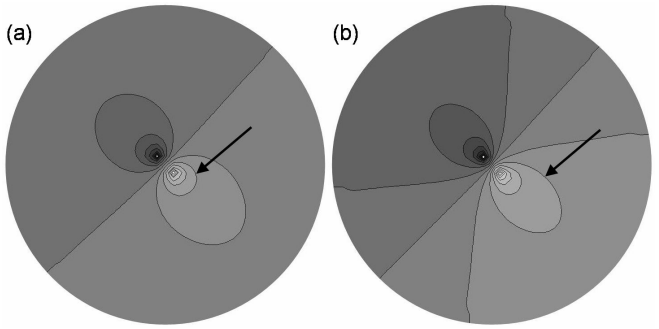

Fig. 5. Electric potential distributions for the (a) isotropic and (b) anisotropic spherical head. The arrows indicate the same isopotential contour line for both distributions. The gray levels, from white to black, represent the range from maximum positive to maximum negative potentials with respect to the zero reference set between the source and sink currents.

Acknowledgment

M. J. D. Cook and Z. J. Koles thank J. C. de Munck for providing the code for the analytic spherical head model.

References

[1] J. Haueisen, D. S. Tuch, C. Ramon, P. H. Schimpf, V. J. Wedeen, J. S. George, and J. W. Belliveau, "The influence of brain tissue anisotropy on human EEG and MEG," *NeuroImage*, vol. 15, pp. 159-166, 2002.

[2] L. A. Neilson, M. Kovalyov, and Z. J. Koles, "A computationally efficient method for accurately solving the EEG forward problem in a finely discretized head model," *Clinical Neurophysiology*, vol. 116, pp. 2302-2314, 2005.

[3] M. G. Edwards, "Symmetric flux continuous positive definite approximation of the elliptic full tensor pressure equation in local conservative form," SPE 29147, presented at the 13th SPE Reservoir Simulation Symposium, San Antonio, TX, 1995.

[4] M. G. Edwards, "Cross flow tensors and finite volume approximation with deferred correction," *Computational Methods in Applied Mechanics and Engineering*, vol. 151, pp. 143-161, 1998.

[5] M. G. Edwards and C. F. Rogers, "Finite volume discretization with imposed flux continuity for the general tensor pressure equation," *Computational Geosciences*, vol. 2, pp. 259-290, 1998.

[6] M. G. Edwards, "Split full tensor discretization operators for general hexahedral grids," *SPE Journal*, pp. 102-108, March 2004.

[7] P. I. Crumpton, G. J. Shaw, and A. F. Ware, "Discretisation and multigrid solution of elliptic equations with mixed derivative terms and strongly discontinuous coefficients," *Journal of Computational Physics*, vol. 116, pp. 343-358, 1995.

[8] H. I. Saleheen and K. T. Ng, "New finite difference formulations for general inhomogeneous anisotropic bioelectric problems," *IEEE Transactions on Biomedical Engineering*, vol. 44, pp. 800-809, 1997.

[9] J. C. de Munck, "The potential distribution in a layered anisotropic spheroidal volume conductor," *Journal of Applied Physics*, vol. 64, pp. 464-470, 1988.